J Solid State Electrochem (2014) 18:2139–2147
DOI 10.1007/s10008-014-2469-0

ORIGINAL PAPER

Facilely prepared polypyrrole-graphene oxide-sodium dodecylbenzene sulfonate nanocomposites by in situ emulsion polymerization for high-performance supercapacitor electrodes

Yunqiang Zhang · Mei Li · Lanlan Yang · Kaihua Yi · Zhen Li · Jinshui Yao

Received: 13 January 2014 / Revised: 19 March 2014 / Accepted: 20 March 2014 / Published online: 2 April 2014

Abstract The layered polypyrrole-graphene oxide-sodium dodecylbenzene sulfonate (PPyGO-SDBS) nanocomposites were facilely fabricated via an in situ emulsion polymerization method with the assistance of SDBS as dopant and stabilizer. Scanning electron microscopy (SEM), transmission electron microscopy (TEM), Fourier transform infrared spectroscopy (FTIR), X-ray diffraction (XRD), and electrochemical performance were employed to analyze the structure and the characteristics of the composites. The results showed that SDBS played an important role in improving the electrochemical performance of the PPyGO-SDBS, by dispersing the PPy between the layers of the GO. The obtained PPyGO-SDBS exhibited remarkable performance as an electrode material for supercapacitors, with a specific capacitance as high as 483 F g^{-1} at a current density of 0.2 A g^{-1} when the mass ratio of pyrrole to GO was 80:20. The attenuation of the specific capacitance was less than 20 % after 1,000 charge–discharge processes, supporting the idea that PPy inserted successfully into the GO interlayers. The excellent electrochemical performance seemed to arise from the synergistic effect between the PPy and the GO and the dispersion of the PPy induced by SDBS.

Keywords PPyGO-SDBS nanocomposites · Supercapacitors · Specific capacitance · Rate capacity · Cycling stability

Y. Zhang · M. Li (✉) · L. Yang · K. Yi · Z. Li · J. Yao
School of Materials Science and Engineering,
Qilu University of Technology, Daxue Road, Western University Science Park, 250353 Jinan, Shandong, People's Republic of China
e-mail: lim@qlu.edu.cn

M. Li
e-mail: plum3lm@aliyun.com

M. Li · J. Yao
Shandong Provincial Key Laboratory of Processing and Testing Technology of Glass and Functional Ceramics, Jinan 250353, People's Republic of China

M. Li · J. Yao
Key Laboratory of Amorphous and Polycrystalline Materials, Qilu University of Technology, Jinan 250353, People's Republic of China

Introduction

During the past few decades, supercapacitors, also known as electrochemical capacitors (ECs), are promising power sources and have been widely used in portable electronics, hybrid electric vehicles, digital communication systems, and uninterrupted power supply of high-power devices [1–3]. Based on the charge-storage mechanism, ECs include pseudocapacitors and electrical double layer capacitors (EDLCs) [4]. Nevertheless, as a precondition for practical application, there are still several pivotal issues for ECs that need to be improved, for example, the rate capability, specific capacitance, cycling stability, cost, etc. [1, 2, 5, 6]. From a materials science point of view, these issues concerning ECs are closely related to the electrode and electrolyte materials used. In order to enhance the property of ECs, most of the research is concentrated on using innovative electrode materials, suitable electrolytes, and tuning the electrolyte/electrode interface performances. The consecutive development of nanometer-sized materials benefits the progress of supercapacitor technologies a lot. Recently, carbon-based nanofillers, such as carbon nanotubes (CNTs), activated carbon, expanded graphite, and graphene (GN), with high surface area have been widely used for ECs [7, 8].

Meanwhile, graphene oxide (GO), a single sheet of graphite oxide, whose edges and basal planes are abundant with various oxygen functional groups (−OH, −COOH, −CHO, epoxy groups), has also attracted great interest. It can be easily prepared in large scales by treating natural graphite with strong aqueous oxidizing agents. Due to its intercalating, superior mechanical, ion-exchange properties and low cost [9–11], it is preferred over other expensive fillers like GN and CNTs. Also, thanks to its abundant oxygen-containing functional groups, GO possesses excellent hydrophilic properties and can therefore be readily dispersed in water. This provides abundant opportunities for the formation of GO-based nanocomposites. So far, several GO-based polymer composites have been developed, and the mechanical, thermal, and electrical properties of these composites were found to be augmented, as reported [12, 13].

Polypyrrole (PPy) is a promising electrode material for ECs with unusual doping/dedoping processes, good electrical conductivity, low cost, environmental stability, and simple synthesis. However, it also exhibits poor stability and rate capability, which limit its wide application [14]. Significantly, composites based on PPy and GO have shown synergetic effects, for example, enhancement in capacitances, stability, electrical conductivity, and electrochemical cyclability [15, 16]. Feng et al. fabricated polypyrrole/modified graphite oxide (PPy/MGO) composites by in situ polymerization and demonstrated that its specific capacitance is 202 F g^{-1} at a current density of 1 A g^{-1} and the capacitance retention of PPy/MGO is 169 F g^{-1} after 1,000 cycles at a scan rate of 1 A g^{-1} [17]. Konwer et al. fabricated PPy/GO composites via in situ polymerization of pyrrole in the presence of GO in various proportions (5 and 10 %). High specific capacitance of the PPy/GO composite of 421.4 F g^{-1} was obtained in the potential range from 0 to 0.80 V at 2 mA current compared with 237.2 F g^{-1} for pure PPy by galvanostatic charge–discharge analysis. Incorporation of GO into the PPy matrix has a pronounced effect on electrochemical capacitance performance of PPy/GO nanocomposites [18]. In most instances, preparation of conducting polymer nanocomposites is conducted by an in situ polymerization technique. But the performance of ECs assembled in this way still has room for improvement as the GO sheets tend to stack together easily in this method, and it has been suggested that these stacks become in fact barriers to electron transport [19, 20].

This work focuses on the combination of the complementary properties of GO and PPy. Herein, careful studies on the intercalation of PPy into layered GO by an in situ emulsion polymerization method in the presence of sodium dodecylbenzene sulfonate (SDBS) have been carried out. First, GO can be delaminated into sheets and dispersed in SDBS aqueous solution to form SDBS-GO (soft-hard) templates. The surfactants intercalated between GO sheets can effectively inhibit aggregation of GO sheets during the process of composition. Then, PPy particles were synthesized via emulsion polymerization and spontaneously assembled onto the GO sheets under the π-π interaction between PPy and the unoxidized domain of GO sheets. To the best of our knowledge, no previous work has been reported for preparing polypyrrole-graphene oxide (PPyGO) composite by using SDBS as a soft template and stabilizer. This method is a more controllable and slower reaction than conventional polymerization techniques. Moreover, it is a facile and novel approach to synthesize bulk quantities of PPyGO nanocomposites. For comparison, PPyGO composites prepared without SDBS and PPy particles alone were prepared using the same method. The obtained PPyGO nanocomposites using SDBS as soft templates exhibited excellent electrochemical and cycling properties.

Experimental

Chemicals

Graphite and SDBS were supplied by Alfa Aesar and Nanjing Chemical Reagent Co. Ltd., respectively. Pyrrole (Py) (98 %) was purchased from Aldrich and distilled under vacuum prior to use. All other reagents were of analytical grade and used as received without further purification.

General characterization

The microstructure and morphology of the samples were observed by a scanning electron microscope (SEM) (Hitachi S-4800) with an acceleration voltage of 5 kV and a transmission electron microscope (TEM) (JEM-2100) with an acceleration voltage of 200 kV, respectively. The Fourier transform infrared spectroscopy (FTIR) spectra were recorded on a TENSOR 27 FTIR spectrometer using KBr pellets. X-ray diffraction (XRD) patterns were obtained on a D8 ADVANCE (Bruker AXS, Germany) using Cu/Ka radiation (λ=1.5406 Å) radiation.

Preparation of graphene oxide

The graphite oxide was prepared from natural graphite powder using a modified Hummers method [21]. For purification, the product was washed several times with 5 % of HCl and distilled water. The product was exfoliated by ultrasonication for 2 h. Finally, a homogeneous GO aqueous dispersion was obtained and used for further preparation of PPyGO-SDBS nanocomposites.

Preparation of PPyGO-SDBS nanocomposites

PPyGO-SDBS nanocomposites were prepared using an in situ emulsion polymerization method with Py and GO in the presence of SDBS. The different mass ratios of Py to GO prepared were as follows: 95:5, 90:10, 85:15, 80:20, 75:25, 65:35, and 50:50. The resulting composites were named as $PPyGO_{ratio}$-SDBS. For example, $PPyGO_{80:20}$-SDBS indicates that the mass ratio of Py to GO is 80:20. In a typical experiment, firstly, 6.5 mmol of SDBS was dissolved in 50 mL of distilled water. The solution was transferred into a three-neck flask and chilled at 0 °C. Then, 0.45 mL of Py was added into the SDBS solution and stirred for 2 h. Secondly, the required amount of GO solution was subjected to ultrasonic treatment for 2 h and added into the above mixture and then stirred at 0 °C for 48 h. Thirdly, 2 g of $FeCl_3 \cdot 6H_2O$ was dispersed in 0.12 M HCl (50 mL) and slowly dropped into the above mixture. The reaction was carried out with stirring for 24 h at 0 °C. Finally, the reaction mixture was filtered, washed with distilled water and ethanol, and dried at 40 °C for 12 h to obtain the $PPyGO_{80:20}$-SDBS composites. For comparison, $PPyGO_{80:20}$ composites without SDBS and PPy particles with SDBS were prepared by the same method.

Electrochemical performance tests

The three-electrode cell system was used to evaluate the electrochemical performance of the prepared electrode materials in 1 M KCl aqueous electrolyte. The working electrode was made by mixing 80 wt% active material, 10 wt% acetylene black, and 10 wt% poly(vinylidene fluoride) in *N*-methyl-2-pyrrolidone, and the slurry was coated onto a 1-cm × 1-cm nickel foam current collector and dried at 40 °C for 8 h to evaporate the solvent. A platinum sheet and a standard calomel electrode (SCE) were used as counter electrode and reference electrode, respectively. Cyclic voltammetry (CV), galvanostatic charge–discharge analysis, and electrochemical impedance spectroscopy (EIS) were conducted using a PARSTAT2263 electrochemical workstation. The electrical conductivity was determined by a four-probe instrument (RTS-8) at room temperature. The samples were compacted into pellets of 15 mm diameter and about 0.5 mm thickness under pressure of 20 MPa.

Results and discussion

The synthesis mechanism of PPyGO-SDBS nanocomposites

The synthesis mechanism of the PPyGO-SDBS nanocomposites is illustrated in Scheme 1. First of all, SDBS formed a mass of micelles in aqueous solution and the Py molecules entered into the above micelles due to its good oil solubility. Secondly, graphite oxide was delaminated into GO nanosheets in the SDBS solution. GO is reported to be uniquely amphiphilic with negatively charged hydrophilic edges and hydrophobic basal plane [22]. SDBS is thought to assemble on the surface of GO sheets through π-π interactions and hydrophobic interactions [23]. Finally, with the addition of $FeCl_3$, PPy particles were synthesized and assembled onto the GO sheets owing to the π-π interaction between PPy and the unoxidized domains of the GO sheets.

Structure and morphology studies

The structure and morphology of GO, PPy particles, $PPyGO_{80:20}$, and $PPyGO_{80:20}$-SDBS were investigated by SEM (Fig. 1) and TEM (Fig. 2). The PPy particles prepared by the emulsion polymerization with SDBS are shown in Fig. 1a. The PPy looks like cauliflower agglomerated with spherical particles. Particle sizes are slightly less than 100 nm. As depicted in Fig. 1b, GO exhibits smoother plates and multilayered lamellar flakes with different sizes stacked together which is consistent with the literatures [24, 25]. In Fig. 1c, the $PPyGO_{80:20}$ agglomerated into big lumps and its layer structure is not obvious as that of the $PPyGO_{80:20}$-SDBS shown in Fig. 1d. A careful inspection of the Fig. 1d suggested that there are some typical characteristics that are worthy of mention. Firstly, the PPy particles seem to be stitched together, and a flaky, rough morphology can be observed on the surface of the GO. Furthermore, the thickness of the obtained composite nanosheets is much thicker than bare GO owing to the depositing and insertion of PPy. Comparing panel d with c of Fig. 1, we can deduce that SDBS plays a pivotal role to disperse the PPy particles between the interlayers of the GO

Scheme 1 The synthesis mechanism of $PPyGO_{ratio}$-SDBS nanocomposites

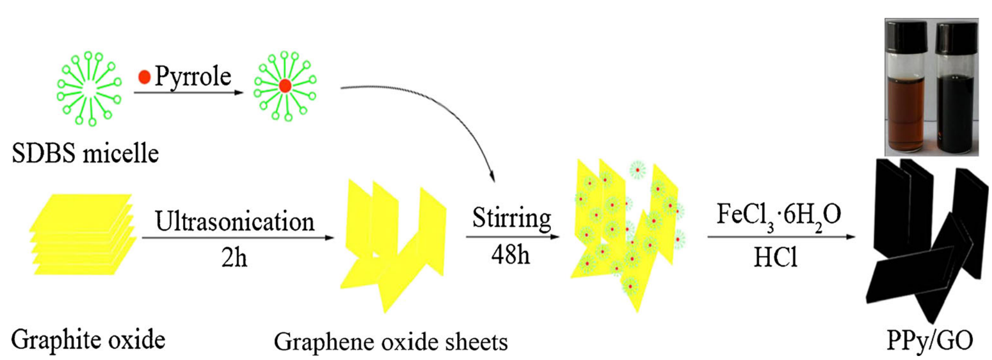

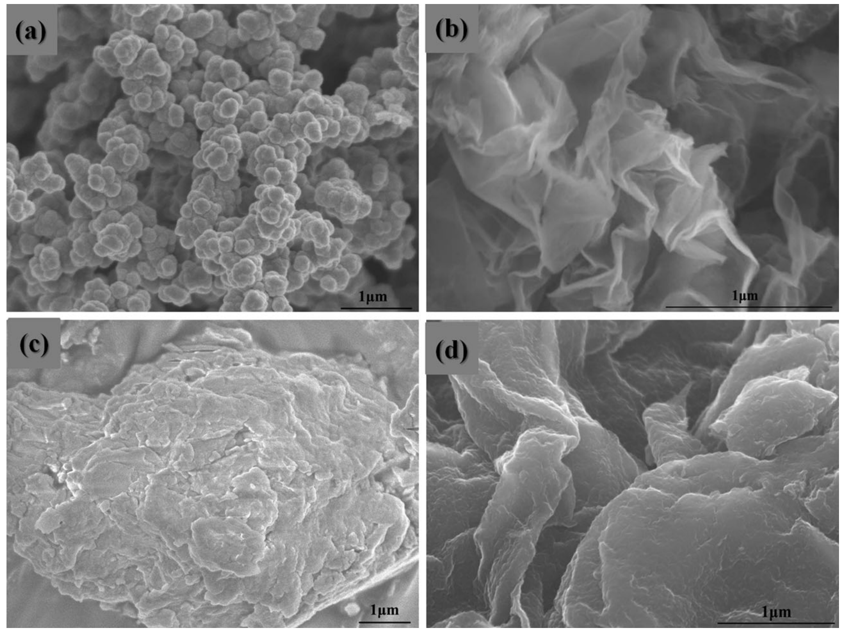

Fig. 1 SEM images of **a** PPy particles, **b** pure GO, **c** $PPyGO_{80:20}$, and **d** $PPyGO_{80:20}$-SDBS

and obtain the more homogeneous composites compared with that without SDBS.

More details can be observed from the TEM images of the different samples. In Fig. 2a, the PPy particles gather together and many lumps could be observed which is consistent with the result of the SEM. In Fig. 2b, GO shows an overlapped lamellar structure and the obvious wrinkle of an individual GO sheet is shown. Compared with Fig. 2b, $PPyGO_{80:20}$-SDBS composites in Fig. 2d are fuzzy and not so smooth as the GO due to the polymerization of PPy covering the surface of the GO sheets, which has been confirmed by the SEM image of Fig. 1d. In Fig. 2c, the PPy particles are deposited between the interlayers of the GO and are not well distributed, so it seems that clusters of PPy particles agglomerated with GO which may influence their electrochemical performance.

The structure and component of the prepared PPyGO nanocomposites were characterized by Fourier transformed infrared (FTIR) spectra and XRD. Figure 3a shows the FTIR spectra of GO, PPy particles, and $PPyGO_{80:20}$-SDBS composites. GO exhibits the following characteristic absorptions, for example, the C=O stretching vibration peak at 1,732 cm^{-1}, the vibration and deformation peaks of O–H groups at 3,386 and 1,417 cm^{-1}, and the C–O (alkoxy) stretching peak at 1,057 cm^{-1} [24, 26]. Compared with GO, several new peaks

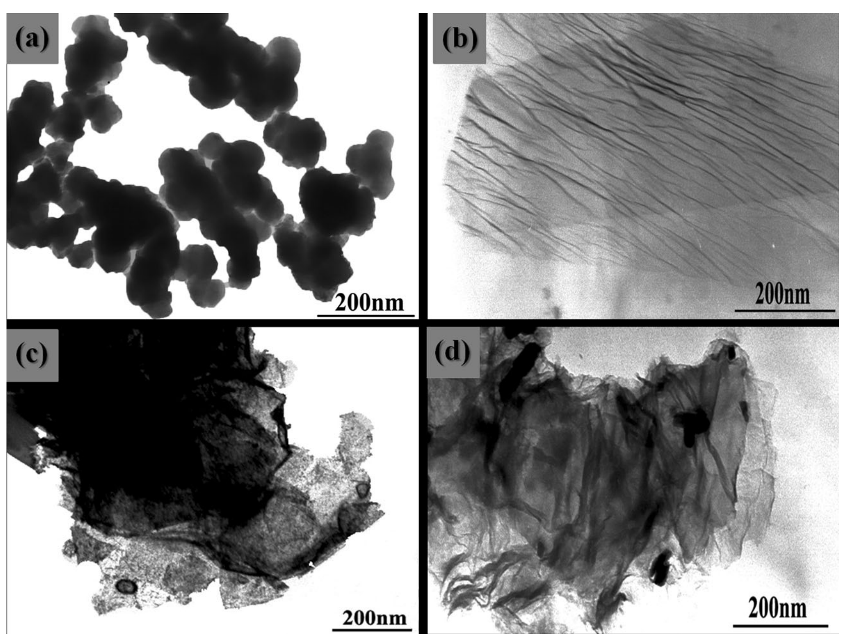

Fig. 2 TEM images of **a** PPy particles, **b** GO, **c** $PPyGO_{80:20}$, and **d** $PPyGO_{80:20}$-SDBS

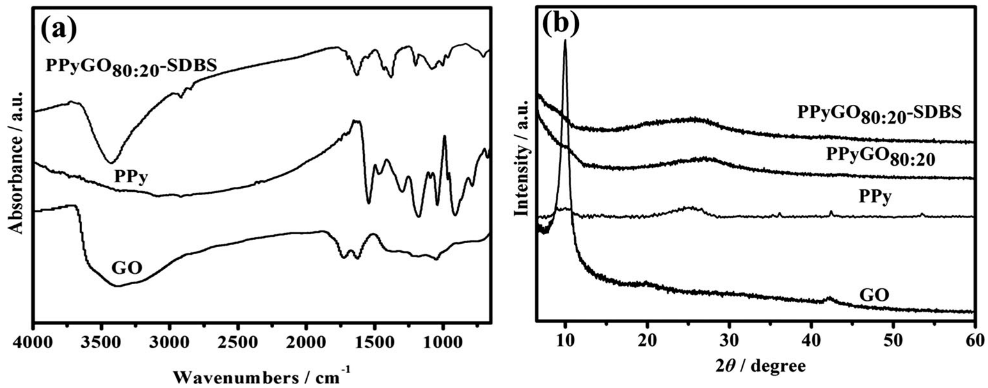

Fig. 3 **a** FTIR spectra of pristine GO, PPy particles, and PPyGO$_{80:20}$-SDBS. **b** XRD patterns of pure GO, PPy particles, PPyGO$_{80:20}$, and PPyGO$_{80:20}$-SDBS

ascribed to PPy appeared in the spectrum of PPyGO$_{80:20}$-SDBS. The new peaks at 1,548, 1,458, and 3,437 cm^{-1} are ascribed to the C–C, C–N, and N–H stretching vibration in the PPy ring. In addition, the bands at 2,925 and 2,851 cm^{-1} attributed to the asymmetric stretching and symmetric vibrations of CH_2 in the SDBS were also observed [27, 28]. It should be remarked that the peak due to the C=O group within the PPyGO$_{80:20}$-SDBS has been downshifted to 1,700 cm^{-1} which is maybe due to the π-π interactions and hydrogen bonding between the GO films and aromatic polypyrrole rings [29, 30]. The obtained PPyGO nanocomposites were further studied by powder XRD measurements, as shown in Fig. 3b. PPy particles exhibit a weak and broad diffraction peak at $2\theta=25.9°$ ($d=0.343$ nm), which indicates that the PPy is amorphous. XRD patterns of the GO showed an intense, sharp peak centered at $2\theta=9.98°$, corresponding to an average interplanar distance (d) about 0.886 nm of the GO. In the case of the PPyGO$_{80:20}$-SDBS and PPyGO$_{80:20}$, because the GO surface has been covered by PPy, the peak at $2\theta=9.98°$ disappeared and the characteristic peak ($2\theta=25.9°$) of PPy becomes much weaker and broader. However, in comparison with PPyGO$_{80:20}$-SDBS ($2\theta=25.9°$), the diffraction peak of PPyGO$_{80:20}$ is weaker and shifts to a higher angle ($2\theta=27.1°$). The interplanar space of PPyGO$_{80:20}$ is about 0.329 nm, a little less than that of the PPyGO$_{80:20}$-SDBS, implying that the interplanar space tends to expand with the assistance of SDBS and the PPy particles entering into the interlayer of GO more easily. This result is confirmed by Figs. 1 and 2.

Electrical properties

Conductivity

The room temperature average conductivities of PPy particles and PPyGO composites are summarized in Table 1. The conductivity of PPy particles prepared by utilizing SBDS as the template is about 0.020 S m^{-1} and that of the obtained PPyGO$_{80:20}$ composites without SDBS is 0.023 S m^{-1}. The value of the above two materials is similar but several orders of magnitude higher than that of GO (1.28×10^{-6} S cm^{-1}) and pure PPy (1.08×10^{-4} S cm^{-1}) without SDBS. Interestingly, PPyGO$_{80:20}$-SDBS shows better conductivity (0.280 S m^{-1}) over ten times greater than the other two samples. The conductivity of the PPyGO$_{80:20}$-SDBS seems to increase with low GO content and upon doping with the SDBS. The doping of PPy with SDBS and composition with GO due to π-π conjugation induces a great increase of the conductivity of the PPyGO$_{80:20}$-SDBS. More importantly, GO was dispersed well in SDBS solution which is beneficial to PPy polymerization between intercalated GO flakes, and GO sheets may serve as a bridge connecting PPy conducting domains and increase its effective percolation. Furthermore, the π-π electron stacking

Table 1 The conductivity, C_{sp}, power, and energy densities of different electrode materials

Sample	Preparation method	Conductivity (σ, S cm^{-1})	C_{sp} (F g^{-1})/current density (A g^{-1})		Power density (W kg^{-1}), energy density (Wh kg^{-1})	Reference
PPy/MGO	In situ polymerization	–	202/1	–	244~1,000, 12.6~8.2	[17]
PG$_{9:1}$	In situ polymerization	–	310/0.5	210/5	55~5,510, 10.5~1.4	[31]
GO/PPy	One-step coelectrodeposition	–	356/0.5	–	–	[32]
PPy	In situ emulsion polymerization	0.020	200/0.5	25/5	55~3,950, 4.95~0.5	This work
PPyGO$_{80:20}$	In situ polymerization	0.023	282.78/0.5	164/5	60~4,500, 29.1~11.5	This work
PPyGO$_{80:20}$-SDBS	In situ emulsion polymerization	0.280	431.15/0.5	315/5	80~6,000, 42.93~22.88	This work

between the Py ring of PPy and unoxidized domain of GO could divert electrons more effectively [28].

EIS analysis

The electrode conductivity and ion-transport kinetics were further characterized by EIS. EIS was recorded in the frequency range from 10^5 to 0.1 Hz at open circuit potential with alternate current amplitude of 10 mV. The resulting Nyquist plots for PPy particles, $PPyGO_{80:20}$, and $PPyGO_{80:20}$-SDBS are shown in Fig. 4. In the region with low frequencies, the slope of the plot for the $PPyGO_{80:20}$-SDBS composites is steeper than that of PPy particles and $PPyGO_{80:20}$, indicating that $PPyGO_{80:20}$-SDBS possesses better capacitive behavior (vertical line for an ideal capacitor) and lower diffusion resistance of ions [33]. In the higher frequency region, the real axis intercept is the equivalent series resistance (R_s), and the radius of the semicircle plotted is indicative of electrode conductivity and the charge transfer resistance (R_{ct}) in the electrode materials [34]. Careful inspection of the plots at higher frequencies reveals that the $PPyGO_{80:20}$-SDBS exhibits a smaller semicircle than PPy particles and $PPyGO_{80:20}$ which illustrated that the $PPyGO_{80:20}$-SDBS had a lower R_{ct} and much faster charge transfer rate. SDBS not only assists PPy to insert successfully into GO interlayers and form the interpenetrating conducting structure, but also enhances surface wettability by electrolytes [35] and, hence, greatly improves the conductivity of the nanocomposites, which is favorable for their supercapacitor applications.

The CV characteristics and galvanostatic charge–discharge analysis

PPy particles, $PPyGO_{80:20}$, $PPyGO_{50:50}$-SDBS, $PPyGO_{65:35}$-SDBS, $PPyGO_{80:20}$-SDBS, and $PPyGO_{95:5}$-SDBS were examined by CV in 1 M KCl aqueous solution in order to test the potential feasibility as supercapacitors. The cyclic voltammetry curves (CVs) with a potential range from −0.2 to 0.6 V at a scan rate of 5 mV s^{-1} are shown in Fig. 5a. All of the samples indicate reasonable symmetrical characteristic except $PPyGO_{80:20}$. In general, compared to PPy particles, the five $PPyGO_{ratio}$-SDBS nanocomposites with different mass ratios have larger electrochemical response currents. It is clear that the response current of $PPyGO_{80:20}$-SDBS is the largest, illustrating that its specific capacitance is the highest, which is consistent with the results of the galvanostatic charge–discharge analysis as shown in Fig. 5d. Moreover, Fig. 5b exhibits the CVs of the $PPyGO_{80:20}$-SDBS composite electrode at different scan rates from 5 to 100 mV s^{-1}. The shapes of CVs show symmetric current-potential characteristics, meaning a high reversibility and efficiency [36]. The increase of current with the scan rates means good rate ability for the $PPyGO_{80:20}$-SDBS electrodes [37]. But the rate ability of $PPyGO_{80:20}$-SDBS still requires improvement, something which will be explored in our further work.

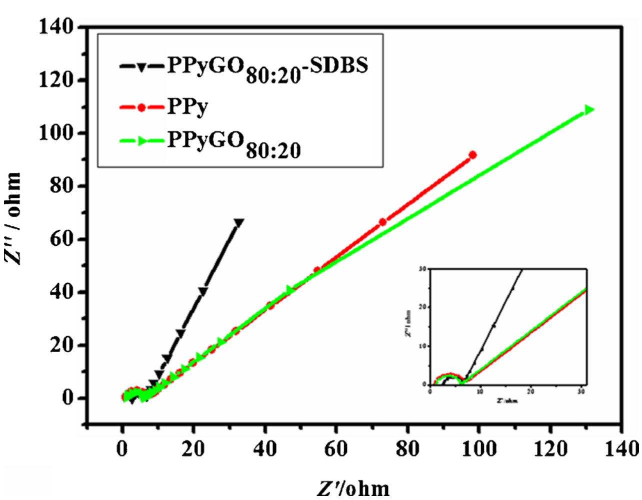

Fig. 4 Nyquist plots of the PPy particles, $PPyGO_{80:20}$, and $PPyGO_{80:20}$-SDBS in 1 M KCl solution measured at open circuit potential

Figure 5c exhibits the galvanostatic charge–discharge curves (GCD) of PPy particles, $PPyGO_{80:20}$, and $PPyGO_{80:20}$-SDBS electrodes at current densities of 0.5 A g^{-1}. The near triangular shape of the curves indicates that the materials have good reversibility. The specific capacitance of the $PPyGO_{80:20}$-SDBS is much higher than that of PPy particles and $PPyGO_{80:20}$ under the same current density, which can be clearly found in Fig. 5c, d. The specific capacitance (C_{sp}) is calculated from the discharge process according to the following Eq. (1) [38]:

$$C_{sp} = (I\Delta t)/(m\Delta V) \quad (1)$$

where C_{sp} is the specific capacitance (F g^{-1}), I is the current (A), Δt is the discharge time (s), m is the mass of active materials in the electrode (g), and ΔV is the potential window (V).

In addition, as shown in Fig. 5d, the C_{sp} for $PPyGO_{80:20}$-SDBS composites is the highest (483 F g^{-1}) among all the samples, which exceeds that of PPy particles (270 F g^{-1}) and $PPyGO_{80:20}$ (364 F g^{-1}), at a discharge current density of 0.2 A g^{-1}. The C_{sp} of $PPyGO_{80:20}$-SDBS composites still remained as high as 315 F g^{-1} even at a high discharge current density of 5 A g^{-1}, while those of PPy particles and $PPyGO_{80:20}$ sharply decrease to 25 and 164 F g^{-1} (Table 1), respectively. It is noted that the $PPyGO_{80:20}$-SDBS composites show not only high specific capacitance but also better rate capability, demonstrating that the 80:20 ratio is the most optimal, of all the samples tested. This result is important and has not been involved in the previous reports concerning the PPyGO nanocomposites [17, 31]. Based on the above

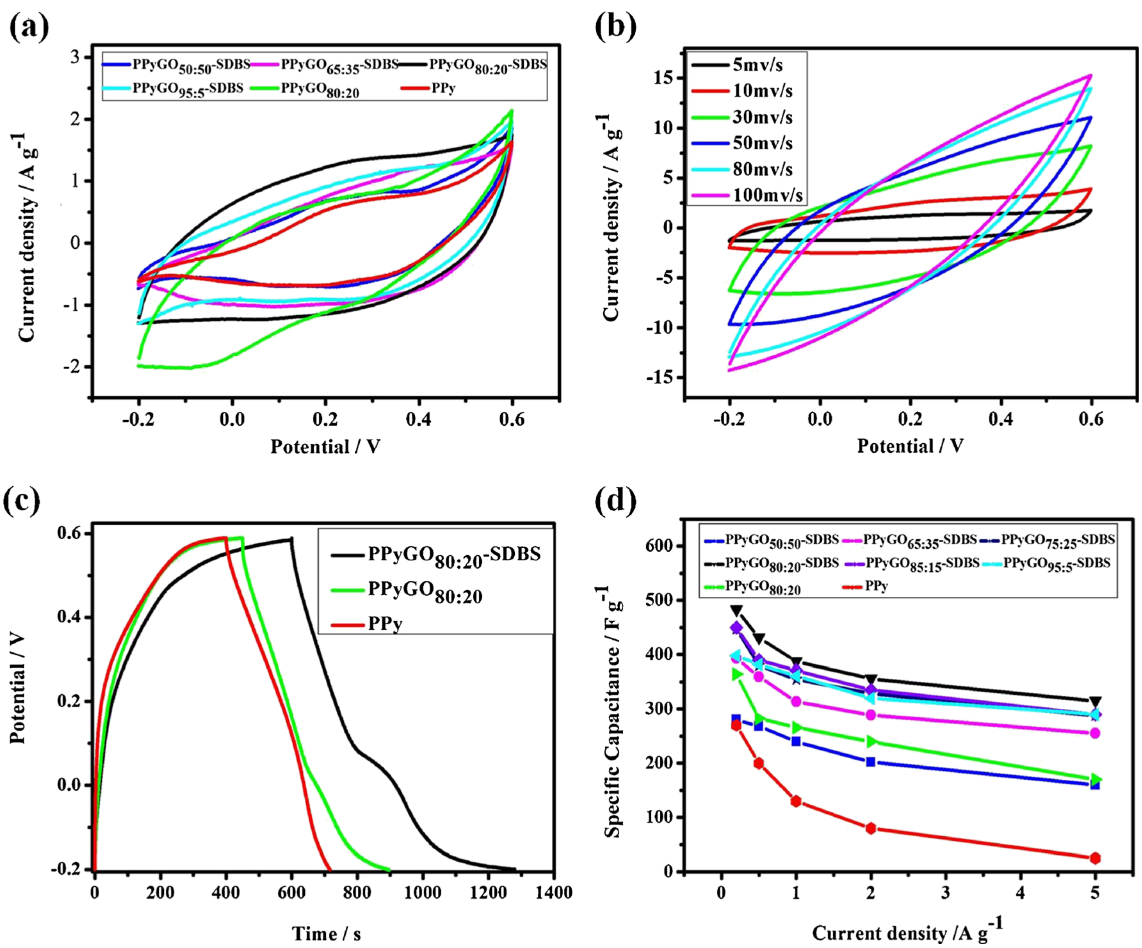

Fig. 5 a CVs of PPy particles, $PPyGO_{80:20}$, $PPyGO_{50:50}$-SDBS, $PPyGO_{65:35}$-SDBS, $PPyGO_{80:20}$-SDBS, and $PPyGO_{95:5}$-SDBS at a scan rate of 5 mV s^{-1}. b CVs for $PPyGO_{80:20}$-SDBS measured at various scan rates. c Galvanostatic charge–discharge curves of PPy particles, $PPyGO_{80:20}$, and $PPyGO_{80:20}$-SDBS at a current density of 0.5 A g^{-1}. d The specific capacitances of PPy particles, $PPyGO_{80:20}$, and $PPyGO_{ratio}$-SDBS electrodes at different current densities. The mass of the sample is 3 mg

discussion, the better rate capability and improved capacitance of $PPyGO_{80:20}$-SDBS might be mainly attributed to the reaction of the SDBS with GO which assisted the complete intercalation of PPy into GO layers to form interpenetrating conducting structure. The obtained $PPyGO_{80:20}$-SDBS had a more homogeneous layer structure compared to that of $PPyGO_{80:20}$, and SDBS is also known to enhance surface wettability [35] and facilitate electron transport and ion insertion/extraction in the electrode material during the quick charge–discharge processes. So out of all the different ratios of PPy/GO tested, $PPyGO_{80:20}$-SDBS nanocomposites exhibited the best electrochemical characteristics such as specific capacitance, rate capability, and cycling stability.

The cycling stability

Long cycling life is another important property for supercapacitors. The electrochemical stability of PPy particles, $PPyGO_{80:20}$, and $PPyGO_{80:20}$-SDBS electrodes is investigated at a current density of 2 A g^{-1}, and the results are shown in Fig. 6a. It is found that there are no significant differences among these three samples at the beginning of 400 cycles. After 1,000 charge–discharge cycles, the specific capacitance of $PPyGO_{80:20}$-SDBS composites still remains 80 % of the initial capacitance, which was much higher than that of PPy particles (50 %) and $PPyGO_{80:20}$ (66 %), indicating good cycling stability of $PPyGO_{80:20}$-SDBS as electrode material. The great performance of the $PPyGO_{80:20}$-SDBS could be attributed to the following two reasons: (1) The addition of SDBS is favorable for GO to delaminate and PPy to deposit on the surface of GO. The homogeneous PPyGO-SDBS nanocomposites reduce the strain associated with the volume change of PPy during the charge–discharge processes and, hence, avoid the destruction of the electrode material. (2) SDBS enhanced the surface wettability and accelerated the electron transport and ion insertion/extraction in the electrode material during the quick charge–discharge processes [35].

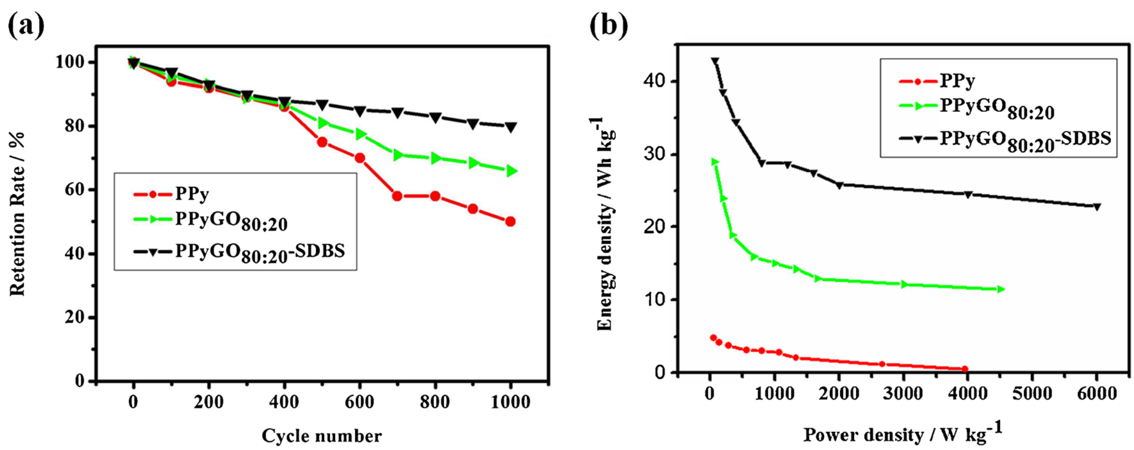

Fig. 6 **a** Cycle stability of PPy particles, $PPyGO_{80:20}$, and $PPyGO_{80:20}$-SDBS electrodes from the 1st to the 1,000th cycle at a current density of 2 A g^{-1}. **b** Ragone plots of PPy particles, $PPyGO_{80:20}$, and $PPyGO_{80:20}$-SDBS

The Ragone plot analysis

A Ragone plot is used to compare the performance of various energy-storing devices [39]. The energy density and power density of $PPyGO_{80:20}$-SDBS, $PPyGO_{80:20}$, and PPy in the three-electrode system are estimated from galvanostatic discharge curves at different currents and marked in the Ragone plot, as shown in Fig. 6b. The energy density values of $PPyGO_{80:20}$-SDBS electrode are in the range of 42.93~22.88 Wh kg^{-1}, while the power density values are in the range of 80~6,000 W kg^{-1}, revealing that there is a decrease in energy density of the electrode material with an increase of power density. Compared with $PPyGO_{80:20}$-SDBS, $PPyGO_{80:20}$, and PPy electrodes, the energy density of $PPyGO_{80:20}$-SDBS is the highest under the same power density. Moreover, we provided power and energy densities of similar structured electrode materials (Table 1), to compare with our sample ($PPyGO_{80:20}$-SDBS). Obviously, power and energy densities of the $PPyGO_{80:20}$-SDBS are much higher than that of the similar electrode materials prepared by in situ polymerization. Based on the excellent electrochemical properties, the PPyGO-SDBS nanocomposites could be applied as electrode materials for electrochemical supercapacitors.

Conclusions

PPyGO-SDBS composites have been successfully prepared which exhibit excellent electrochemical characteristics including high specific capacitance, great rate capability, and cycling stability. SDBS acting as stabilizer and dopant played an important role in facilitating PPy particles to enter into interlayers of GO. The specific capacity of the obtained $PPyGO_{80:20}$-SDBS composites was up to 483 F g^{-1} at a current density of 0.2 A g^{-1} and retained above 80 % after 1,000 charge–discharge processes. Further optimization and control of the structures to develop better electrochemical properties of GO-based composites are under investigation in our lab.

Acknowledgments This study was supported by the College Scientific Plan Fund of Shandong Education Department (J10LD23) and the Doctoral Startup Foundation of Qilu University of Technology (12042826).

References

1. Miller JR, Simon P (2008) Electrochemical capacitors for energy management. Science 321:651–652
2. Winter M, Brodd RJ (2004) What are batteries, fuel cells, and supercapacitors? Chem Rev 104:4245–4269
3. Fuertes AB, Lota G, Centeno TA, Frackowiak E (2005) Templated mesoporous carbons for supercapacitor application. Electrochim Acta 50:2799–2805
4. Simon P, Gogotsi Y (2008) Materials for electrochemical capacitors. Nat Mater 7:845–854
5. Burke A (2000) Ultracapacitors: why, how, and where is the technology. J Power Sources 91:37–50
6. Zhang LL, Zhao XS (2009) Carbon-based materials as supercapacitor electrodes. Chem Soc Rev 38:2520–2531
7. Gogotsi Y, Simon P (2011) True performance metrics in electrochemical energy storage. Science 334:917–918
8. Kuilla T, Bhadra S, Yao D, Kim NH, Bose S, Lee JH (2010) Recent advances in graphene based polymer composites. Prog Polym Sci 35:1350–1375
9. Dékány I, Krüger-Grasser R, Weiss A (1998) Selective liquid sorption properties of hydrophobized graphite oxide nanostructures. Colloid Polym Sci 276:570–576
10. Bourlinos AB, Gournis D, Petridis D, Szabó T, Szeri A, Dékány I (2003) Graphite oxide: chemical reduction to graphite and surface modification with primary aliphatic amines and amino acids. Langmuir 19:6050–6055
11. Liu N, Luo F, Wu H, Liu Y, Zhang C, Chen J (2008) One-step ionic-liquid-assisted electrochemical synthesis of ionic-liquid-functionalized graphene sheets directly from graphite. Adv Funct Mater 18:1518–1525
12. Zhuang XD, Chen Y, Liu G, Li PP, Zhu CX, Kang ET, Noeh KG, Zhang B, Zhu JH, Li YX (2010) Conjugated-polymer-functionalized graphene oxide: synthesis and nonvolatile rewritable memory effect. Adv Mater 22:1731–1735

13. Liu P, Gong K, Xiao P, Xiao M (2000) Preparation and characterization of poly(vinyl acetate)-intercalated graphite oxide nanocomposite. J Mater Chem 10:933–935
14. Zhang X, Yang W, Ma Y (2009) Synthesis of polypyrrole-intercalated layered manganese oxide nanocomposite by a delamination/reassembling method and its electrochemical capacitance performance. Electrochem Solid-State Lett 12:A95–A98
15. Zhang LL, Zhao S, Tian XN, Zhao XS (2010) Layered graphene oxide nanostructures with sandwiched conducting polymers as supercapacitor electrodes. Langmuir 26:17624–17628
16. Zhang K, Zhang LL, Zhao XS, Wu J (2010) Graphene/polyaniline nanofiber composites as supercapacitor electrodes. Chem Mater 22:1392–1401
17. Feng H, Wang B, Tan L, Chen N, Wang N, Chen B (2014) Polypyrrole/hxadecylpyridinium chloride-modified graphite oxide composites: fabrication, characterization, and application in supercapacitors. J Power Sources 246:621–628
18. Konwer S, Boruah R, Dolui SK (2011) Studies on conducting polypyrrole/graphene oxide composites as supercapacitor electrode. J Electron Mater 40:2248–2255
19. Gu Z, Zhang L, Li C (2009) Preparation of highly conductive polypyrrole/graphite oxide composites via in situ polymerization. J Macromol Sci B 48:1093–1102
20. Gu Z, Li C, Wang G, Zhang L, Li X, Wang W, Jin S (2010) Synthesis and characterization of polypyrrole/graphite oxide composite by in situ emulsion polymerization. J Polym Sci B Polym Phys 48:1329–1335
21. Li Y, Wu Y (2009) Coassembly of graphene oxide and nanowires for large-area nanowire alignment. J Am Chem Soc 131:5851–5857
22. Kim J, Cote LJ, Kim F, Yuan W, Shull KR, Huang J (2010) Graphene oxide sheets at interfaces. J Am Chem Soc 132:8180–8186
23. Chang H, Wang G, Yang A, Tao X, Liu X, Shen Y, Zheng Z (2010) A transparent, flexible, low-temperature, and solution-processible graphene composite electrode. Adv Funct Mater 20:2893–2902
24. Zhu C, Guo S, Fang Y, Dong S (2010) Reducing sugar: new functional molecules for the green synthesis of graphene nanosheets. ACS Nano 4:2429–2437
25. Zhu C, Guo S, Fang Y, Han L, Wang E, Dong S (2011) One-step electrochemical approach to the synthesis of graphene/MnO_2 nanowall hybrids. Nano Res 4:648–657
26. Zhu C, Guo S, Wang P, Xing L, Fang Y, Zhai Y, Dong S (2010) One-pot, water-phase approach to high-quality graphene/TiO2 composite nanosheets. Chem Commun 46:7148–7150
27. Bose S, Kim NH, Kuila T, Lau KT, Lee JH (2011) Electrochemical performance of a graphene-polypyrrole nanocomposite as a supercapacitor electrode. Nanotechnology 22:295202–295210
28. Bose S, Kuila T, Uddin ME, Kim NH, Lau AKT, Lee JH (2010) In-situ synthesis and characterization of electrically conductive polypyrrole/graphene nanocomposites. Polymer 51:5921–5928
29. Bora C, Dolui SK (2012) Fabrication of polypyrrole/graphene oxide nanocomposites by liquid/liquid interfacial polymerization and evaluation of their optical, electrical and electrochemical properties. Polymer 53:923–932
30. Li L, Xia K, Li L, Shang S, Guo Q, Yan G (2012) Fabrication and characterization of free-standing polypyrrole/graphene oxide nanocomposite paper. J Nanoparticle Res 14:1–8
31. Zhang D, Zhang X, Chen Y, Yu P, Wang C, Ma Y (2011) Enhanced capacitance and rate capability of graphene/polypyrrole composite as electrode material for supercapacitors. J Power Sources 196:5990–5996
32. Zhu C, Zhai J, Wen D, Dong S (2012) Graphene oxide/polypyrrole nanocomposites: one-step electrochemical doping, coating and synergistic effect for energy storage. J Mater Chem 22:6300–6306
33. Pandey GP, Hashmi SA, Kumar Y (2010) Multiwalled carbon nanotube electrodes for electrical double layer capacitors with ionic liquid based gel polymer electrolytes. J Electrochem Soc 157:A105–A114
34. Pandey GP, Hashmi SA, Kumar Y (2010) Performance studies of activated charcoal based electrical double layer capacitors with ionic liquid gel polymer electrolytes. Energy Fuels 24:6644–6652
35. Zhang K, Mao L, Zhang LL, Chan HSO, Zhao XS, Wu J (2011) Surfactant-intercalated, chemically reduced graphene oxide for high performance supercapacitor electrodes. J Mater Chem 21:7302–7307
36. Li L, Qiu J, Wang S (2013) Three-dimensional ordered nanostructures for supercapacitor electrode. Electrochim Acta 99:278–284
37. Wang YG, Li HQ, Xia YY (2006) Ordered whiskerlike polyaniline grown on the surface of mesoporous carbon and its electrochemical capacitance performance. Adv Mater 18:2619–2623
38. Wang G, Huang J, Chen S, Gao Y, Cao D (2011) Preparation and supercapacitance of CuO nanosheet arrays grown on nickel foam. J Power Sources 196:5756–5760
39. Jaidev RS (2012) Poly(p-phenylenediamine)/graphene nanocomposites for supercapacitor applications. J Mater Chem 22:18775–18738